Journal of Marine Systems
July 2019, Volume 195, Pages 50-66
https://doi.org/10.1016/j.jmarsys.2019.03.008
https://archimer.ifremer.fr/doc/00487/59904/

Lagrangian pathways in the southern Benguela upwelling system

Ragoasha Natalie [1, 2, *], Herbette Steven [1], Cambon Gildas [5], Veitch Jennifer [1], Reason Chris [3, 4], Roy Claude [5]

[1] Laboratoire dOcéanographie Physique et Spatiale (LOPS), IUEM, Univ. Brest - CNRS - IRD - Ifremer, Brest, France
[2] Department of Oceanography, University of Cape Town, South Africa
[3] SAEON, Egagasini Node, Cape Town, South Africa
[4] Nansen-Tutu Centre, Marine Research Institute, Department of Oceanography, University of Cape Town, South Africa

* Corresponding author : Natalie Ragoasha, email address : rgsmoa001@myuct.ac.za

Abstract :

The effect of ocean currents on fish eggs and larvae during their journey from spawning to nursery grounds in the Southern Benguela upwelling system is poorly understood. The survival and successful transport of fish eggs and larvae results from complex biological and physical processes. This study focuses on the advective processes, more specifically on how the dynamics and characteristics of the ocean currents shape the Lagrangian pathways in the Southern Benguela. A mesoscale eddy resolving interannual (1989–2010) simulation of the region, with a horizontal resolution of 7.5 km, is used to study processes impacting the connectivity between the western edge of the Agulhas Bank and the west coast upwelling region. A set of Lagrangian experiments are conducted with particles being released within the top 100 m of the water column along an across-shore transect off Cape Point (34◦ S). Transport success is given by the ratio of the number of particles that reach St Helena Bay (32◦ S) over the total number of particles released. The model results show a strong seasonal cycle in transport success which is governed by the complex three-dimensional structure of the along-shore jets, their variability, together with the wind-induced Ekman drift. Transport success is most efficient in spring when the Benguela Jet consists of one coherent intensified single-core branch that flows over the 300 m isobath, and when wind-induced Ekman transport favours the retention of particles within the jet. At this time of the year, the pathway leading to successful transport is located inshore, with 90% of particles released inshore the 300 m isobath being successfully transported to St Helena Bay in <15 days. This pathway is also characterized by low eddy kinetic energy values.

During the upwelling season (December–March), transport success becomes less efficient, and less sensitive to the initial across-shore position of the particles. The inshore route no longer dominates, as the majority of particles follow offshore pathways. The Benguela Jet shifts offshore and splits into several branches due to the shoaling of the poleward undercurrent. The entrainment of particles within the offshore branch of the jet is favored by the dominating offshore wind-induced Ekman transport. Particles trapped in the offshore branch get exposed to higher mesoscale variability. Their northward progression is slower, which leads to journeys generally exceeding 20 days.

This study shows that successful transport from the Agulhas Bank to the west coast upwelling region cannot be attributed to only a simple wind induced modulation of the jet. It explores how the seasonal modulation of the Benguela Jet, poleward undercurrent and offshore Ekman transport combine together with the turbulent off-shelf eddy field to set-up the characteristics of transport success.

Highlights

► Fish larvae pathways in the Southern Benguela Upwelling System ► A 300 miles along shore fast route for fish larvae in the Southern Benguela ► Lagrangian pathways in the Southern Benguela Upwelling System

Keywords : Benguela, Upwelling, alongshore connectivity, Lagrangian pathways, coastal jet, poleward undercurrent

1. Introduction

In the southern Benguela upwelling system (SBUS), anchovy spawn in austral spring over the Agulhas Bank, a 200 m deep large coastal plateau that extends south of the tip of the African continent (Hutchings, 1992). The nursery area[1] is located off the west coast of southern Africa, 400 km north of the spawning area. This makes the SBUS distinctive from its northern Benguela counterpart and the other major eastern boundary upwelling systems (EBUS) for which spawning and nursery grounds overlap. In their early-stage, anchovy larvae have minimal swimming ability, which makes them behave as passive particles. Therefore, their dispersion and transport, from the Agulhas Bank to the nursery area, are directly dependant on the oceanic circulation (Pagès et al., 1991).

Hutchings (1992) presented a schematic picture of the major processes impacting the eggs and larvae journey from the western Agulhas Bank to the west coast upwelling region (Fig. 1). This scheme was based on knowledge of the coastal circulation and on numerous observations of eggs and larvae distribution (Bang and Andrews, 1974; Shelton and Hutchings, 1982; Shannon, 1985; Armstrong et al., 1987; Shelton and Hutchings, 1990). A coastal current flowing northward and following the shelf, namely the Benguela Jet, is considered as the major conveyor belt linking the western Agulhas Bank and the west coast upwelling area.

According to Nelson (1989), the Benguela Jet is a narrow current ($\sim$ 20 km) that flows northward along the South African west coast between Cape Point (34.15° S, 18.4° E) and Cape Columbine (33° S, 17.5° E). The jet can sustain high velocities, ranging from 25 cm.s^{-1} to 75 cm s^{-1} (Bang and Andrews, 1974;

[1]The nursery is defined as the region where fish larvae, in their advanced-stage, find a suitable habitat for their growth.

Gordon, 1985). It lies over a poleward undercurrent (Nelson and Hutchings, 1983), that flows over the shelf edge and occasionally reaches the surface. The jet varies in position and strength, and responds rapidly to changes in wind stress magnitude and direction. It follows the seasonal cycle of the upwelling (Armstrong et al., 1987) and intensifies in summer when coastal upwelling of cold waters contributes to reinforce the across-shore density gradient (Veitch et al., 2006, 2017). In winter, when the wind direction reverses, this across-shore density gradient weakens, but persists due to the intrusions of warm Agulhas waters from the South (Twatwa Mhlongo et al., 2005).

Hutchings' (1992) scheme for Lagrangian transports of fish eggs and larvae has been widely used to set-up numerous Lagrangian modelling studies in the Southern Benguela (Mullon et al., 2003). Huggett et al. (2003), followed by Parada et al. (2003; 2008), carried out pioneering work demonstrating that the dominant anchovy spawning patterns in the Southern Benguela could be reproduced when combining a 3D hydrodynamic model with a Lagrangian particle-tracking tool. They also quantified the impact, on eggs and larvae transport success, of parameters such as the initial location, density and patchiness of eggs, as well as behavioral processes such as diurnal vertical migration, mortality due to lethal temperatures or predation. However, neither the local pathways nor the physical processes responsible for the transport of particles were studied in detail, despite the fact that the success of their experiments was obviously linked to the capacity of the hydrodynamical model to reproduce the main characteristics of the currents in the region.

The modelling works of Veitch et al. (2006) and Blanke et al. (2009) provided insights on the importance of the Benguela Jet for the connectivity between the western Agulhas Bank and the west coast upwelling area. More recently, in a detailed modelling study of the shelf edge currents, Veitch et al. (2017) de-

scribed the bifurcation of this Jet between Cape Point and Cape Columbine into a weak narrow branch flowing over the shelf edge and a strong offshore branch flowing in the northwestward direction. A bifurcation of the jet, as well as other physical processes such as induced offshore Ekman transport and occasional entrainment by Agulhas rings, have been suggested as important physical processes impacting the alongshore transit of fish eggs and larvae (Hutchings et al., 1998; Skogen et al., 2003; Veitch et al., 2006; Garavelli et al., 2012).

This work builds upon these recent physical modelling studies to investigate in details how the horizontal and vertical structure of the shelf edge jets and the presence of mesoscale turbulence impact the along-shore trajectory of passive particles in the SBUS. The approach consists in a set of Lagrangian particles tracking experiments based on a robust hydrodynamical model capable of simulating the major physical processes influencing the along-shore transport of particles, *i.e.* a realistic seasonal coastal circulation, a realistic mesoscale eddy field, Agulhas leakage bringing warm Agulhas waters offshore of the Benguela shelf.

While our study remains motivated by questions related to the dynamics of anchovy reproductive patterns and to recruitment variability, it distinguishes from the others as it focuses on the physical transport processes that impact the survival of individuals at early stages, whereas previous studies mainly focused on the sensitivity to biological processes (Lett et al., 2015). The Lagrangian experiments are built upon the pioneering work of Huggett et al. (2003) to focus exclusively on the northward alongshore portion of the hypothesized trajectory of anchovy larvae from the Agulhas Bank to St Helena Bay, *i.e.* the portion between Cape Point and St Helena Bay. If the Benguela Jet is assumed to play a dominant role in the transport of fish larvae, the success of this route should be in theory more predictable than the cross-shelf transport in the vicinity of

the turbulent Agulhas retroflection.

A first step towards elucidating the role of the jet consists of identifying the different physical processes that control the seasonal cycle of this northward alongshore connectivity between Cape Point and St Helena Bay, just north of Cape Columbine. The Lagrangian experiments aim at addressing the following: (1) the identification of the dominant pathways that ensure this connectivity; (2) their characteristics and robustness;(3) the ocean dynamics that link to the alongshore transport success seasonal variability. Unlike the climatologically forced model of Veitch et al. (2017), our ocean model is forced by 6-hourly surface forcing (wind, heat and freshwater fluxes) over the 1989-2010 period. The use of a 20 year simulation forced with a realistic non filtered wind field that conserves its full interannual, seasonal and intraseasonal variability gives robustness to our conclusions regarding the role of each individual process on the transport success of particles.

The outline of the paper is as follows. The numerical model and the Lagrangian experiments designed for the purpose of this study are presented in section 2. This section also includes an evaluation of the model's realism by comparing simulated and observed sea surface temperature (SST) and eddy kinetic energy (EKE). Section 3 characterizes the seasonal cycle of the alongshore connectivity in terms of duration of travel and initial positions. The Lagrangian pathways taken by particles are identified in section 4 while section 5 investigates the link between the observed Lagrangian dispersal patterns and the across-shore structure of the ocean circulation, mainly the alongshore currents and the mesoscale turbulent eddy field. Finally, a summary and discussion of our results highlight the complexity of the across-shore structure of alongshore jet currents in the region.

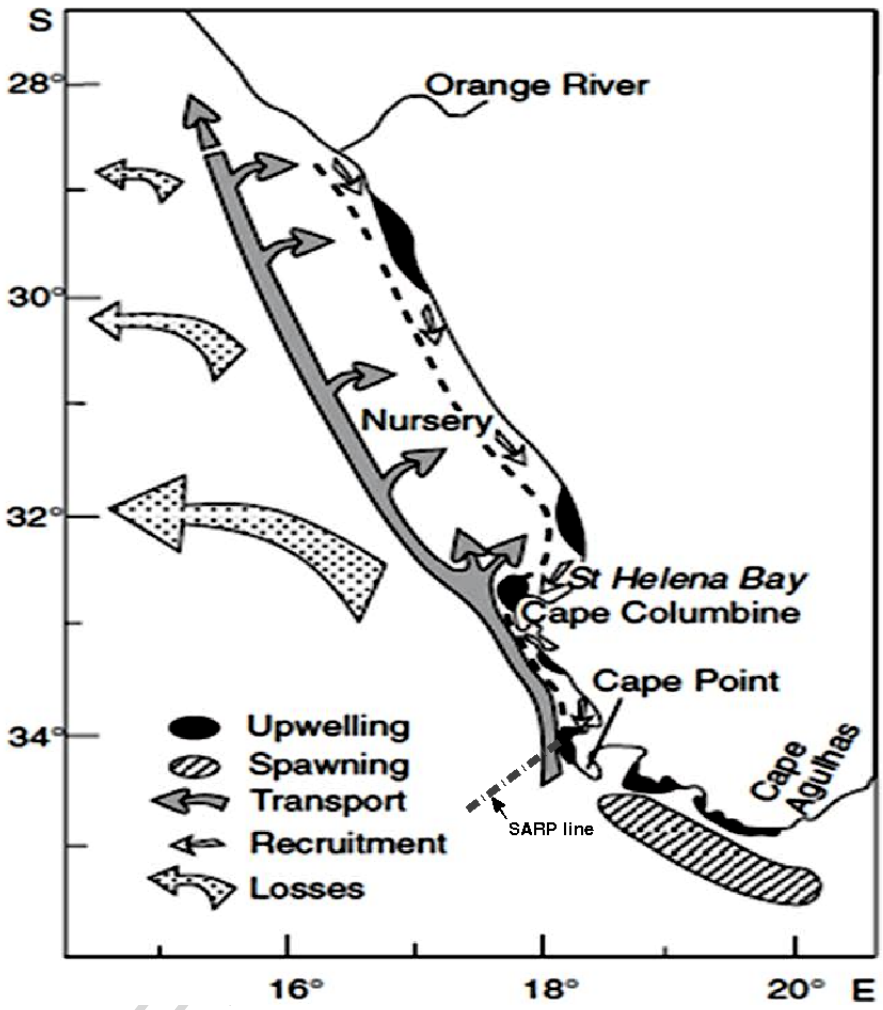

Figure 1: A conceptual diagram of the life history of anchovy in the southern Benguela. Fish eggs are spawned at the tip of Cape Agulhas, and then advected northward alongshore. They experience offshore losses along their way to the west coast. From Hutchings et al. (1998).

2. Data and methodology

2.1. Numerics

This study uses the Regional Ocean Modelling System (ROMS; Shchepetkin and McWilliams, 2005) in its Coastal and Regional Ocean Community

(CROCO) version (Penven et al., 2006; Debreu et al., 2012). ROMS is a free-surface, terrain-following σ-coordinate model with split-explicit time stepping and with Boussinesq and hydrostatic approximations. The advection scheme is third-order upstream biased, which reduces dispersion errors, essentially enhancing precision for a given grid resolution (Shchepetkin and McWilliams, 1998). The diffusive part of the advection scheme is rotated along the isopycnal surfaces to avoid spurious diapycnal mixing (Marchesiello et al., 2009; Lemarié et al., 2012). Adaptive open boundary conditions combine outward radiation and nudging towards prescribed external boundary conditions (Marchesiello et al., 2001). Additional eddy viscosity is added in the sponge layer at open boundaries, where it increases smoothly over several grid points. Subgrid-scale vertical mixing is governed by a non-local, K-profile parametrization (KPP) scheme (Large et al., 1994). A quadratic bottom drag is applied.

A large regional configuration, "BENGR15", extending from 54.5° S to 4.75° S and from 2.5° W to 55.16° E, with a spatial resolution of 1/15° ($\sim$ 7.5km) and 100 vertical levels is developed for this study. The vertical grid is stretched for increased boundary layer resolution using stretching surface and bottom parameters of h_{cline} = 300 m, θ_b = 6, and θ_s = 5. The bottom topography is extracted from the Shuttle Radar Topography Mission (SRTM 30 plus) dataset (available at `http://topex.ucsd.edu/WWW.html/srtm30.plus.html`) and interpolated on the model grid. The SRTM 30 plus product is based on the 1-min Smith and Sandwell (1997) global dataset and higher-resolution surveys when available. In order to avoid pressure gradient errors induced by terrain-following (sigma) coordinates in shallow regions with steep bathymetry, the model bottom topography is smoothed where the steepness of the topography ($r = \frac{\delta h}{2h}$) exceeds 0.2 (Beckmann and Haidvogel, 1993). When the depth is shallower than 10 m, it is reset to 10 m. At the surface, BENGR15 is bulk-forced (Fairall

et al., 1996) with the interannual NCEP Climate Forecast System Reanalysis (CFSR) from 1979 to 2010 (Saha, 2010), with a 6 hourly sampling and a spatial resolution of 0.3°. The conditions for temperature, salinity, horizontal velocity and sea level at the lateral boundaries were provided by a monthly seasonal climatology derived from the SODA 2.3.2 reanalysis (Carton and Giese, 2008). The forcing, initial and boundary conditions were linearly interpolated on the model grid using ROMSTOOLS (Penven et al., 2008). For the purpose of this work, the 1989-2010 period is considered in order to let the oceanic circulation reach a statistical equilibrium. Only a portion of the whole domain, covering the oceanic region surrounding southern Africa, is used (Fig. 2). Velocity components (u, v, w), temperature and salinity fields were averaged and stored every 3 days.

2.2. Evaluation of the model's realism

In order to study the path of passive particles, it is essential that our model reproduces the seasonal cycle of the main currents within the region, as well as a statistically consistent mesoscale eddy field. Sea surface heights from the model and altimetry (AVISO: `http://marine.copernicus.eu/services-portfolio/access-to-products/`) show that the general climatological characteristics of the large scale ocean circulation are well reproduced in our simulation (Fig. 2). The complex and chaotic dynamics of the Agulhas Current and its retroflection, that in turn leads the leakage of warm Indian ocean waters into the Atlantic, is well represented. The Agulhas Current flows south-westward following the east coast of South Africa. When it passes the tip of the Agulhas Bank, it abruptly veers eastward and forms the Agulhas return Current. Although the simulated retroflection tends to occur 100 km east from the observed position, the levels of mean eddy kinetic energy (EKE) found in the model and observations are similarly high within this region. The retroflection is in fact accompanied by

the shedding of large anticyclonic eddies and filaments, some of which enter into the South Atlantic Ocean and form the Agulhas leakage (Loveday et al., 2014). The signature of this leakage in the form of a tongue of high EKE values, spreading northwestward into the Atlantic, can be seen in the model as in the observations. Finally, the long term average of this mesoscale eddy field propagating northwestward into the South Atlantic results in the eastern branch of the South Atlantic subtropical gyre.

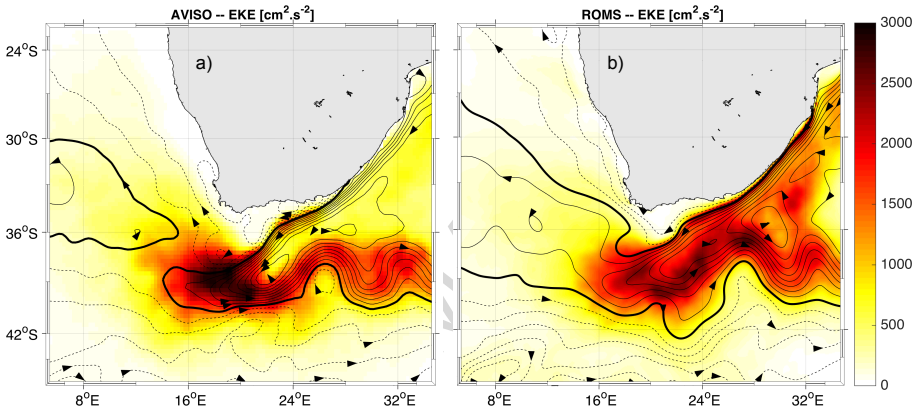

Figure 2: Annual mean surface geostrophic eddy kinetic energy ($\mathrm{cm}^{-2}\mathrm{s}^{-2}$) and contours of sea surface height (cm) from: a) satellite AVISO data (1993-2015); b) model outputs (1989-2010). Contours are plotted every 10 cm in solid/dashed for positive/negative values and arrows represent the orientation of the surface geostrophic flow. A 0.5 cm offset is added to the model data so that maximum values coincide in both plots.

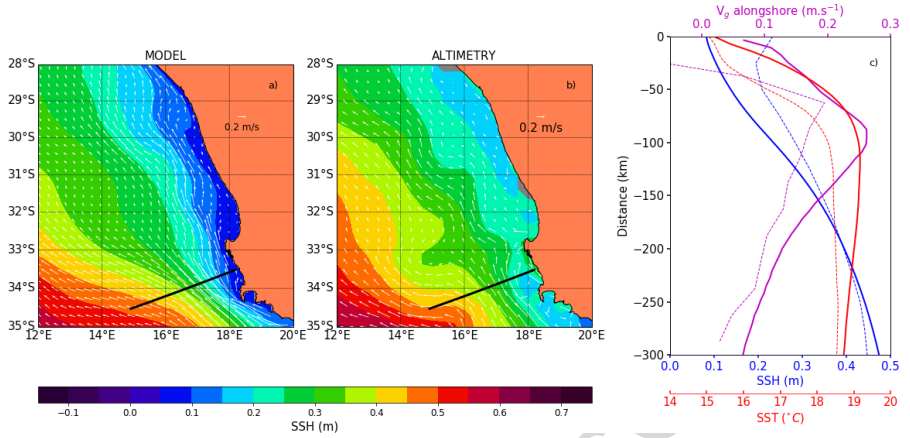

Figure 3: Annual average of sea surface height (SSH) with corresponding surface geostrophic currents superimposed: a) model outputs averaged over 1989-2010; b) satellite absolute dynamic topography (ADT) data averaged over 1993-2010; c) across-shore profiles of model (solid) and satellite (dashed) annual averages of SST (red), ADT (blue) and along-shore geostrophic current (magenta) off Grotto Bay (black line in a) and b). The plotted model SSH was offset by +0.407 m so that the model and satellite spatially average fields matched over the domain of interest.

Zooming in Fig. 2 over the SBUS to get a closer view of the along-shore current shows that the modelled surface geostrophic currents match the observations (Fig.3 a,b). The eastern branch of the South Atlantic subtropical gyre flows northwestward. There is an intensified inshore branch, between the 200 and 500 m isobaths, the Benguela Jet, with average velocities reaching 20 cm s^{-1} in the model, and slightly less (15 cm s^{-1}) in the observations (Fig.3 c). However, this bias could be linked to the coarse resolution of altimetry near the coast. The comparison of the modelled and infrared ODYSEA (Piollé and Autret, 2011) sea surface temperature (SST) shows that the cooling of coastal waters in summer consistently occurs in the model and observations (Fig. 4). There is an inshore warm bias of roughly 1.5^{o}C in the simulation, but such

bias in regional models of EBUS is quite common[2]. In addition, this warm bias is quite homogeneous in its across-shore ($\simeq$ 200 km) and vertical ($\simeq$ 10 m) extension (Fig. 5). Therefore, the surface layers across-shore density gradients are fairly well reproduced in the simulation, and, consequently, the modelled along-shore geostrophic currents derived from the hydrography also match the observations (Fig. 5). In accordance with the results of Veitch et al. (2017), the core of the Benguela Jet in our simulation coincides with the position of the across-shore SST front (Fig. 3, c). Its intensity is also coherent with the estimation from altimetry.

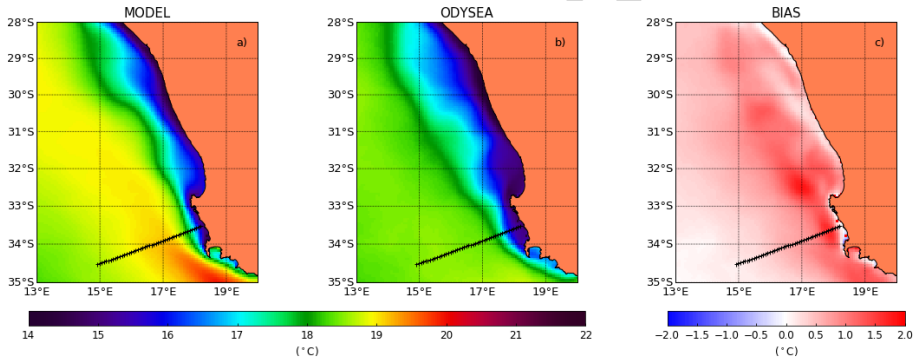

Figure 4: Annual average of Sea Surface Temperature (SST): a) satellite derived infrared data averaged over 2010-2017 (ODYSSEA); b) model data averaged over 1989-2010; c) Annual average of the SST bias (SST_{model} - SST_{ODYSEA}).

[2] Misrepresentation of surface heat fluxes, wind-stress and vertical mixing in the coastal region could partially explain this bias.

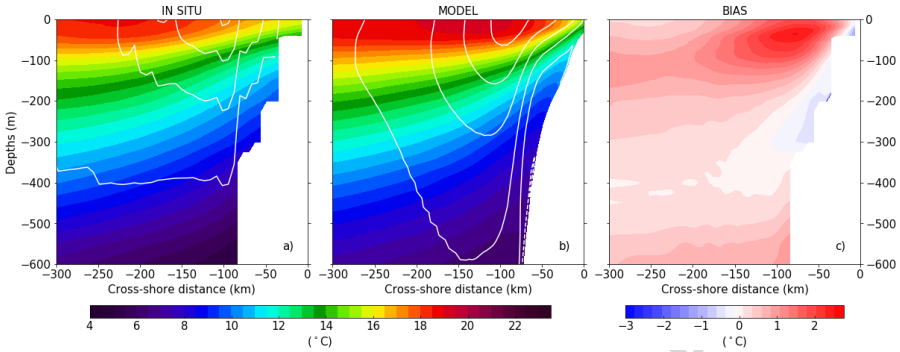

Figure 5: Temperature transect off Grotto Bay (solid black line on Fig. 4) with the along-shore component of the geostrophic current superimposed (white contours). a) World Ocean Atlas annual average (WOA20913); b) Same as in a) for the model; c) Temperature bias (T_{model} - T_{WOA}). Geostrophic velocities is built with a reference level at 1000 m depth. Contours are plotted every with 0.05 m s^{-1} in the range [-0.05 0.25] m s^{-1}. Negative values are dashed.

2.3. Lagrangian particle-tracking experimental setup

In order to study the alongshore connectivity between Cape Point and St Helena Bay, Lagrangian particles are released over 15 defined vertical profiles spaced every 8 km along an across-shore transect situated off Cape Point (Fig. 6a). This transect, located at the southern edge of the Benguela upwelling region, has been intensively sampled during the successive phases of the South African Sardine and Anchovy Recruitment Program (SARP) (Fowler and Boyd, 1998; Huggett et al., 1998). It extends from the coastline at (34° S, 18.4° E) to the 3000 m isobath at (34.15° S, 17.55° E). For each vertical profile, particles are randomly distributed over the first 100 m of the water column with a density of 1.125 particles per meter, which leads to 1845 particles launched simultaneously at each release event. Particles are released every 12 hours from 1989 to 2010 and followed for 30 days using an offline tracking algorithm called Pyticles (Gula et al., 2014). The particles are purely passive, meaning that their spatio-temporal distributions are solely dependent on the 3-dimensional ocean

currents. Particles are advected with a 4th order explicit Runge-Kutta time stepping. No additional diffusion is applied. Particle velocities are interpolated both in time and space from the 3 daily average outputs of the hydrodynamical model using a linear method for the time and vertical interpolation, and a bilinear method for the horizontal interpolation. Numerical discrepancies may occur when the Courant-Friedrichs-Levy (CFL) condition is violated ($\Delta t < \delta x_i/|u_i|$, with Δt the time step, Δx_i the grid resolution along the axis x_i, and $|u_i|$ the absolute value of the x_i velocity component). In our simulations, considering the high vertical resolution (100 vertical levels), CFL violations were most likely to occur for the vertical advection in waters very close to the coast. However, using a time step of 720 s and 3 daily average velocities was sufficient to ensure no CFL violations occurred in the Southern Benguela region.

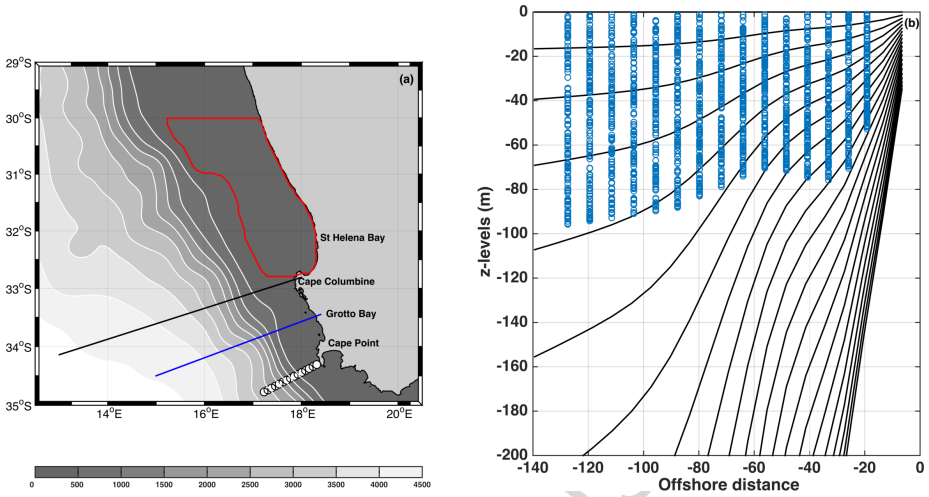

Figure 6: (a): Set-up of the Lagrangian experiments: particles are released every 12 hours over the SARP line (white circles), a across-shore transect off Cape Point. They are counted as successfully transported particles if they reach, within 30 days, the St Helena Bay target area delineated by the red polygon. The bathymetry of the "BENGR15" model (in grey with white contours every 500 m) is also superimposed as well as two other across-shore transects that particles will cross while being advected northward: the Grotto Bay line at 33.5° S (thick blue) and the Cape Columbine line at 33° S (thick black). (b): Initial distribution of particles over the SARP line for a given release event. σ layers are superimposed (black solid).

A particle is considered as successfully transported if it reaches, within 30 days, the St Helena Bay target area. This area is defined as a polygon that extends from the coast to the 300 m isobath and from 32.8° S to 30° S (Fig. 6). For a given release event e, transport success TS_e (Eq. 1) is calculated as the ratio of the number of particles (n_e) that reach the target area over the number of particles released during the event (here 1845).

$$\mathrm{TS}_e = \frac{n_e}{1845}. \tag{1}$$

When a particle exits and re-enters the target area several times within its 30 days life span, it is only counted once at its first entry. This transport success can

also be interpreted as the probability for a particle to be successfully transported from Cape Point to St Helena Bay.

3. Characteristics of the alongshore connectivity

The following section intends to characterize the seasonal cycle of the alongshore connectivity between the SARP line and St Helena Bay in terms of: i) transport success, ii) time taken by successful particles to travel northward, iii) initial vertical and across-shore position of successful particles.

Fig. 7 plots the monthly climatology of the alongshore wind stress at the SARP line together with transport success TS_m and its standard deviation. Both monthly alongshore transport success and its standard deviation show a strong seasonal cycle, that does not strictly superimpose with the upwelling. Upwelling favourable winds prevail in austral spring and summer from October to March, whereas transport success peaks in November-December (late spring), at the beginning of the upwelling season. Our results show that, on average, during this period, particles have a 30% chance of reaching St Helena Bay with a standard deviation as high as 10%. The likelihood of particles making it northward decreases during the peak of the upwelling season (January-February), and reaches its lowest value (13%) in autumn. At this time of the year, the variability of the transport success also appears to be the lowest.

The age of arrival into the target area also varies seasonally (Fig. 8a). There is a peak in the age distribution around 7 days for particles released between July and October. For the rest of the year, the age distribution flattens and gradually shifts towards higher values during the upwelling season. From February to June, it is homogeneously spread between 10 and 25 days. The cumulated histogram of monthly transport success for 4 groups of particles built according to their age of arrival (group I: age$<$10 days; group II: 10$<$age$\leq$15 days; group

III: 15<age≤20 days; group IV 20<age≤30 days) reveals that particles arriving within 10 days account for more than 50% of the successful particles between August and November (Fig. 8b). Particles having short connection time are found all year round but are a minority in late summer and autumn. This suggests the existence of a "fast route" between the SARP line and St Helena Bay, which could be the dominant pathway in late winter and spring. Nevertheless, other routes could exist. There might even be a "slow route" from January to June, when the majority of particles belongs to group IV.

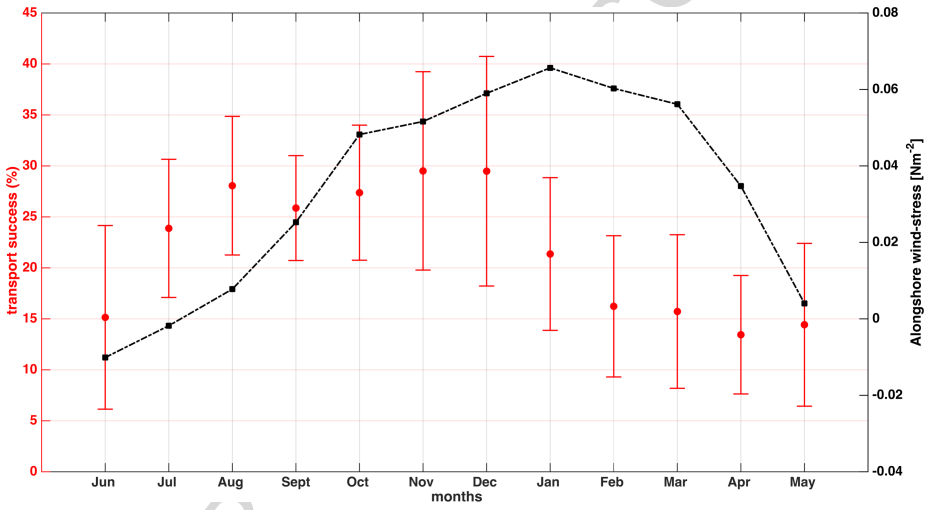

Figure 7: Monthly climatology of transport success TS_m (red dots) and alongshore wind-stress at the SARP line (black dots). The standard deviation of $TS_m$is also superimposed as errorbars. The wind stress is averaged over a box encompassing the Southern Benguela from 12° E to 20° E and 26° S to 36° S.

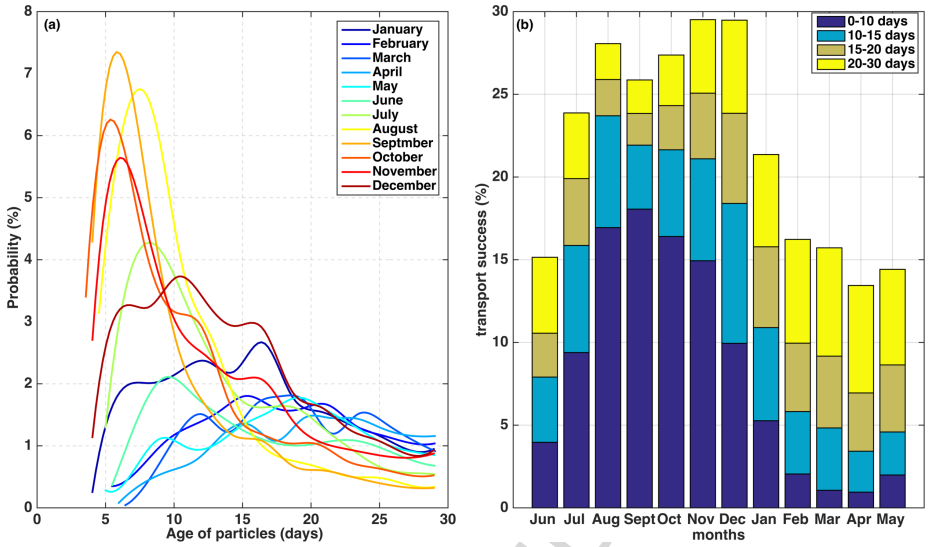

Figure 8: (a): Monthly distribution of successful particles by age when entering the target area. (b): Cumulated histogram of monthly climatology transport success with clusters of particles built according to their age of arrival: group I (age<10 days); group II (10<age≤15 days); group III: (15<age≤20 days); group IV: (20<age≤30 days). Probability have been normalized by the total number of particles released for each month m ($m = 1, \cdots, 12$) over the 22 years of the model run.

The initial vertical and across-shore positions of particles are also important parameters affecting transport success. The majority (∼90%) of particles arriving in St Helena Bay are released between 0 m and 70 m depth (Fig. 9a). There is a peak in the distributions around 55 m depth, whose intensity varies seasonally and intensifies in between October-March. Within this depth range, there is a pronounced seasonal contrast. During austral winter, particles released in the top surface layer (0 to 35 m depth) have a higher probability of reaching St Helena Bay than during the rest of the year (∼ 3.7% in July versus 1.7% in January). If only particles successfully transported are counted in the calculation, 50% of those arriving in St Helena Bay in July are those initially released within the top surface layer. The proportion drops to 25% for those

released in January. During spring and summer, the opposite pattern is observed with particles released in the subsurface layers having a higher transport success. These results are consistent with the general assumption that, in eastern boundary upwelling systems (EBUS), upwelling favourable winds usually enhance the offshore advection of surface particles.

Grouping particles according to the isobath on which they have been released is a way to investigate how the contrasted across-shore structure of the circulation at the SARP line impacts transport success. Particles released over the continental shelf (between the coast and the 300 m isobath) account for more than 50% of the successfully transported particles, although they only represent one sixth of the total number of particles released (Fig. 9b). Their probability of reaching St Helena Bay gets as high as 75% (not shown) in late winter and early spring. Further investigations (not shown) indicate that being released inshore not only increases the particles' probability to reach St Helena Bay, but also decreases its travel duration.

These results suggest the existence of an efficient "fast" inshore route connecting the western edge of the Agulhas Bank to the west coast upwelling region. However, this analysis is only based on the final and initial positions of the particles. The identification of the pathways taken by these particles is done in the following section by considering the northward progression of particles during their 30 day life span and their average trajectories.

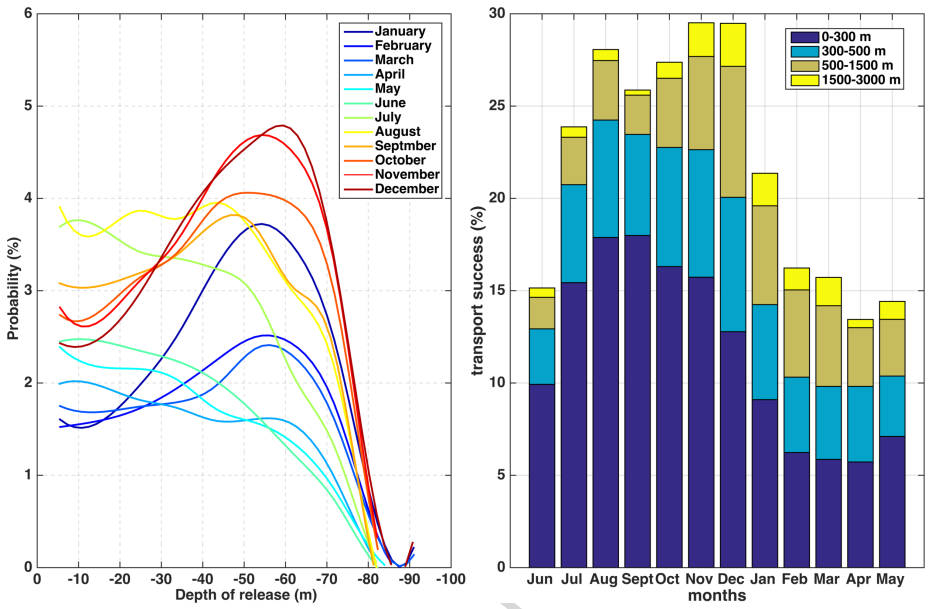

Figure 9: (a): Monthly distribution of successful particles by their depth of release. (b): Cumulated histogram of monthly climatology transport success with clusters of particles built according their initial isobath. Probability have been normalized as in Figure 8.

4. Alongshore Lagrangian pathways

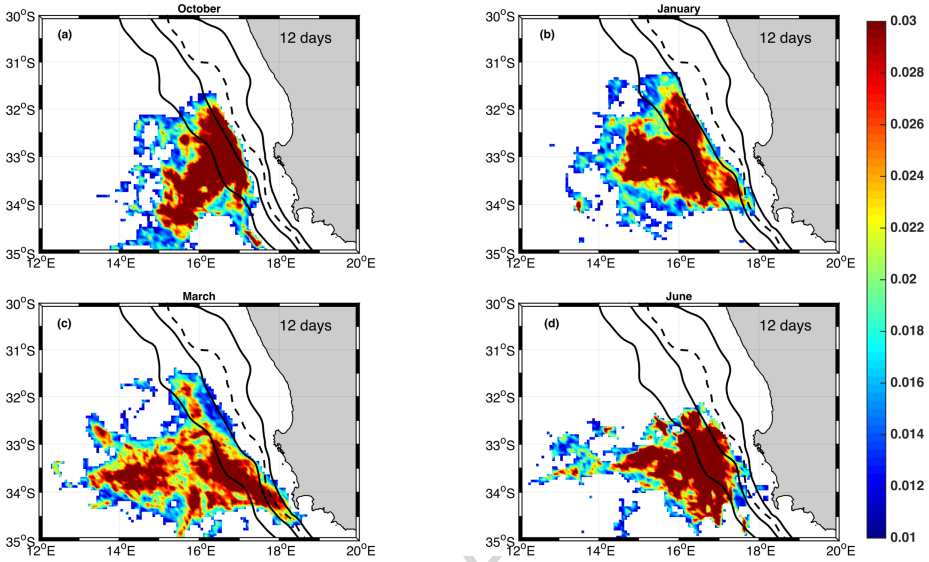

Figure 10: Horizontal distribution of unsuccessful particles (plumes) 12 days after their release for the months of: (a) October; (b) January; (c) March; (d) June. The 200 m, 300 m (dashed), 500 m and 2000 m isobaths are superimposed. The colorbar shows the probability of finding a particle aged 12 days within the water column at a specific grid cell.

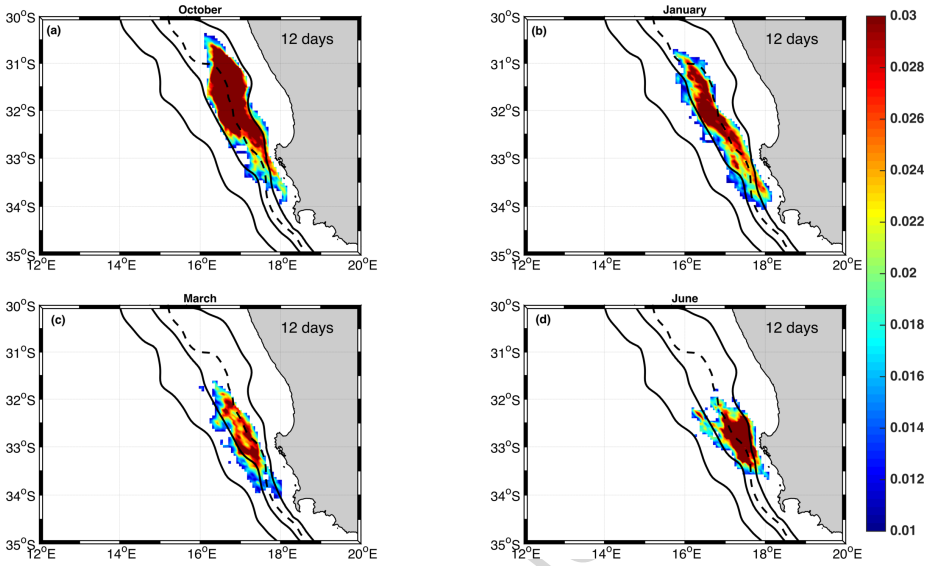

Figure 11: Same as Fig. 10 for the successful particles. The sum of probabilities over the grid gives the transport success plotted in Fig. 7.

In order to get a general view of the routes taken by Lagrangian particles, maps of particles' spatial distribution (plumes) are plotted according to their age τ (in days) on the horizontal grid of the "BENGR15" simulation. The age of particles is zero when they are released. For a series of release events, we count all particles aged τ found within the water column of the grid cell located at position (x, y) in Cartesian coordinates. After dividing this by the total number of particles released during this list of events, we obtain the probability $d(x, y, \tau)$ of finding a particle aged τ at location (x, y). We also build a monthly climatology of this probability. For example, the monthly probability of January is obtained by considering all release events that occurred in January over 1989-2010.

Maps of the spatial distribution of the particles show that, once released on the SARP line, successful and unsuccessful particles take distinct routes. 12 days after their release, unsuccessful particles have been largely spread off-

shore beyond the 500 m isobath (Fig. 10), whereas successful particles remain trapped on the shelf edge between the 200 m and 500 m isobath (Fig. 11). The characteristics of the plume change seasonally. In October, successful particles get dispersed in a compact and elongated plume, that stretches quickly towards the equator following the shelf edge. Additionally, most of these particles make their journey in less than 10 days after being released inshore of the 300 m isobath. From January to June, the northward extension of the plume progressively reduces.

The fate of unsuccessful particles is to be dispersed offshore, following a north-westward orientated cone that extends throughout the coastal transition zone (Fig. 10). They experience a widespread dispersion into the open ocean as they leave the shelf slope region and are advected through the coastal transition zone, an area known for intense mesoscale turbulence in EBUS (Marchesiello et al., 2003; Capet et al., 2008a). The north-westward spreading of unsuccessful particles is maximum in March. The low values of transport success found at this time of the year (Fig. 7) confirm the general idea that passive particles, once advected offshore, struggle to come back inshore. From January to June, the plume also shows a V-shape, past Cape Columbine, which suggests a branching of the route. One branch seems to follow the slope whereas the other bifurcates offshore, as was already pointed out in the work of Garavelli et al. (2012) and Veitch et al. (2017).

A monthly climatology of the successful particles' trajectories is presented in figure. 12. The latter is computed after joining together the geometric centre of the plume of successful particles every 12 hours from 0 to 30 days. This figure highlights the seasonal changes of the pathways taken by successful particles during their transit to St Helena Bay. In January and March, the trajectory of particles is shifted offshore. It starts bending westward at the latitude of the

SARP line, crosses the 500 m isobath, and finally veers back inshore towards the 500 m isobath at Cape Columbine. The majority of successful particles make their journey in more than 20 days (Fig. 8) and follow an offshore path. In October, the offshore route to St Helena Bay is no longer active. The majority of particles make their journey in less than 10 days following an inshore route that almost overlies the 300 m isobath. In June, the few particles reaching St Helena Bay also follow an inshore route, but the latter is slower than during October. Our findings on the seasonality of the pathways and their locations can be summarized as follows. The inshore route is the dominant pathway in late winter and early upwelling season, when offshore Ekman transport is moderate and particles are able to remain inshore. This inshore route is characterized by short connection times (< 10 days). During the peak of the upwelling season, this inshore route persists, but becomes less efficient, as it mainly concerns subsurface particles located below the Ekman layer (about 40 m in the Benguela upwelling system). Connection times also tend to be longer (> 10 days). A slower offshore route, with connection times in the 20-30 days range, exists for particles either initially released on the shelf slope (from the 300 m to the 1500 m isobaths) or advected offshore by Ekman transport during their early age. This offshore route becomes the dominant pathway in summer.

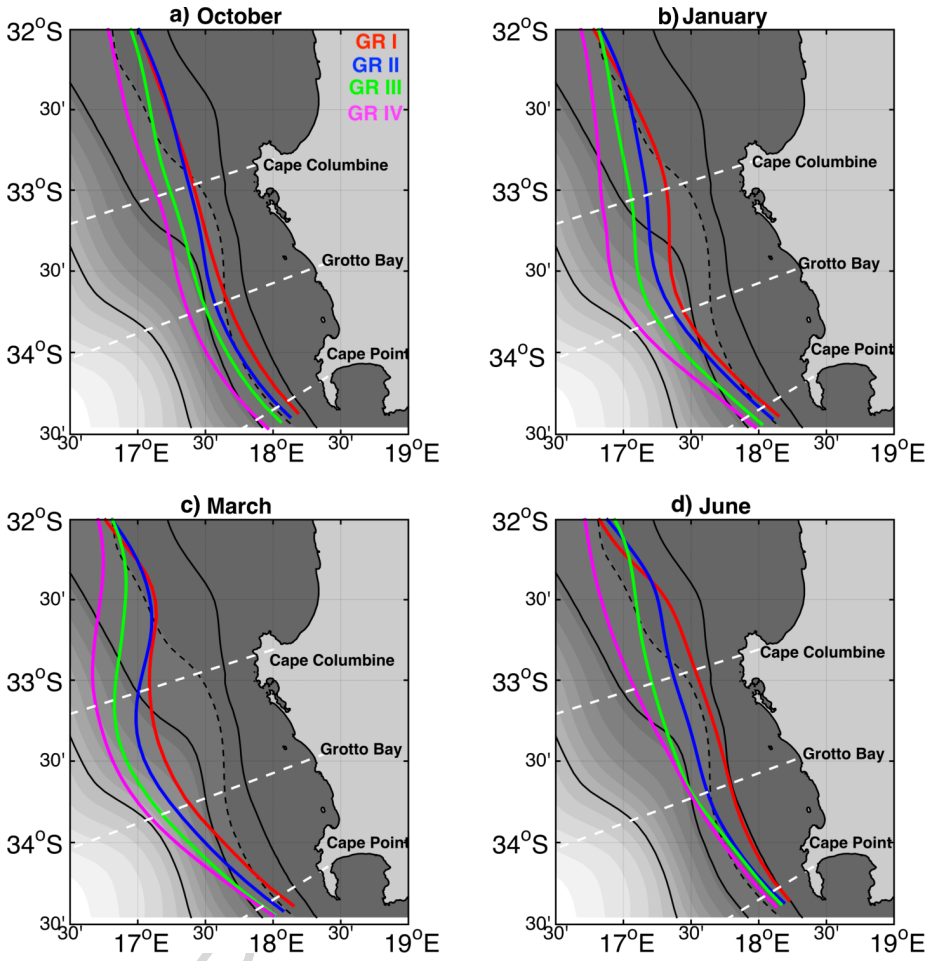

Figure 12: Monthly climatology of the trajectory of successful particles by age of arrival into the target area τ (in days). Trajectories are plotted for particles released in: (a) October; (b) January; (c) March; (d) June. Colours refer to the clusters of particles built according to their age of arrival τ. Group I: $\tau < 10$ (red); Group II: $10 < \tau \leq 15$ (blue); Group III: $15 < \tau \leq 20$ (green); Group IV: $20 < \tau \leq 30$ (magenta). The 200 m, 300 m (dashed), 500 m and 2000 m isobaths are superimposed (black). Note that the mean of the four trajectories at 12 days corresponds to the geometric centre of the plume plotted in Fig. 11. The SARP, Grotto Bay and Cape Columbine lines described in Fig. 6 are also superimposed (white dashed).

5. Inferring the role of the ocean circulation on the Lagrangian pathways

5.1. Characteristics of the ocean surface circulation

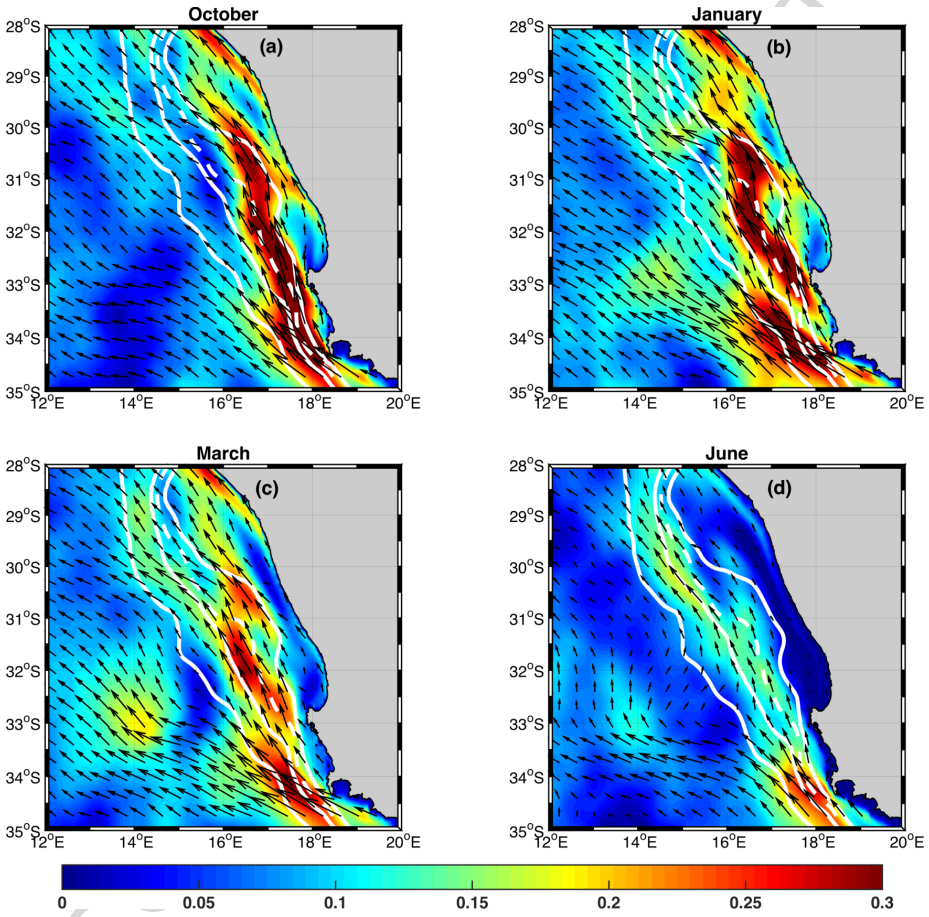

Figure 13: Monthly climatology of surface currents for: (a) October; (b) January; (c) March; (d) June. The magnitude of the current is shown in color (m s^{-1}) and current vectors are superimposed, as well as the 200 m, 300 m (dashed), 500 m and 2000 m isobaths (solid white).

The Lagrangian experiments show that a "fast" inshore route and a "slow" offshore route co-exist and bring particles from Cape Point to St Helena Bay.

The following section investigates how the Eulerian oceanic circulation of the model relates to these identified pathways.

Maps of monthly climatological surface currents show a nearshore equatorward jet, namely the Benguela Jet (Fig. 13). This jet can be observed all-year round, with a marked seasonal variability. In October, it is intensified and spatially coherent. In January, at the vicinity of 33.5° S, it separates into two branches: i) an offshore branch that flows northwestward beyond the 2000 m isobath; ii) a coastal branch that flows alongshore in between the 200 m and 500 m isobaths and intensifies north of Cape Columbine. During the late upwelling season and early winter (March-June), the jet is still separated into two branches, but weakens, except off Cape Point (34° S).

Considering that the Benguela Jet dynamically connects the south and the west coasts of South Africa (Garavelli et al., 2012; Veitch et al., 2017), we superimpose, along three across-shore transects, the across-shore profiles of the: i) distribution of the particles; ii) depth-integrated (top 100 m) alongshore velocity; iii) depth-integrated (top 100 m) eddy kinetic energy (EKE). The across-shore profiles are plotted for the SARP line along which particles are released (Fig. 14), for the transect off Grotto Bay that intersects particles' trajectory at midway (Fig. 15) and for the transect off *Cape Columbine* (Fig. 16) that intersects particles' trajectory just before they enter the target area. The across-shore profile of the distribution of particles is obtained by counting particles crossing the transects. Quantities are normalized by their maximum value found among the 12 monthly climatology across-shore profiles of all three transects (Fig. 12).

Off Grotto Bay and Cape Columbine, the peak in the across-shore distribution of all particles (blue solid) almost superimposes with the peak in the jet's alongshore intensity (red solid). As expected, all year round, particles leave the SARP line and propagate northward embedded within the Benguela Jet. A different

pattern is observed when only successful particles are considered. During their northward progression, successful particles (blue dashed) always remain on the inshore (cyclonic) side of the jet, following roughly the 300 m isobath. This area generally coincides with low values of surface EKE. The EKE can be interpreted as a proxy for the intensity of mesoscale oceanic turbulence. One would expect a particle that goes through an area of strong EKE to be more likely caught within mesoscale turbulent oceanic features, such as eddies and filaments. An exception to this pattern is the occurrence of a secondary peak of EKE nearby the peak of successful particles in October off Grotto Bay (Fig. 15a). However, it does not have a negative effect on transport success because the alongshore jet and/or the topographic slope may be strong enough to counteract the turbulence dispersive effect in the near-shore region. In January and March, when the jet shifts offshore, presumably to conserve its potential vorticity as it gains cyclonic relative vorticity from the wind stress curl (Castelao and Barth, 2007), the peak in all particles also shifts offshore. This results in more particles entering a region where the surface EKE increases from low values at the coast to high values offshore.

At this stage of the analysis, the ability for particles to remain on the inshore side of the jet seems to be a necessary ingredient for transport success. Consequently, one would expect physical processes like wind-induced offshore/inshore Ekman transport during the upwelling/non-upwelling season to have a negative/positive effect on transport success. However, the picture is not as simple. This analysis brings to light that the broadening, the cross-isobath shift and the branching of the jet are other important processes that impact the alongshore connectivity between Cape Point and Cape Columbine, together with wind-induced Ekman transport. During the upwelling season, in January and March, despite intensified offshore Ekman transport, the broadening of the jet

allows most particles to remain embedded within its core up to Grotto Bay (Fig. 15). Off Cape Columbine, multiple alongshore narrow jets exist all year round (Fig. 16). Ekman transport may either make particles follow one particular branch (January), or push them out of any branch (March). In March, the few successful particles are those trapped within the intensified inshore branch of the jet. In June, the distribution of the particles is disconnected from the jet (Fig. 15d). This can result from the inshore Ekman transport induced by prevailing westerly winter winds. It allows successful particles to remain trapped within the cyclonic inshore side of the jet up to Grotto Bay. Further north, when the jet divides into several branches, only the few most inshore particles manage to remain trapped within the inshore branch. The other ones get ejected from any branch, not even reaching the second less offshore branch. The across-shore position of particles at the location of the jet's division seems to be a crucial parameter that determines which branch particles may follow. Wind-induced Ekman velocities may set up this position.

Finally, our results underline the importance of intrusions of Agulhas waters. Off Cape Point, where particles are released, there is a strong variability in the across-shore structure of the alongshore jet (not shown). A significant proportion of particles (30%) is advected southward just after being released, and then advected back northward through the transect. During their return northward path, they may cross the transect at a more offshore position than their initial position, which explains the mismatch (Fig. 14) between the initial distribution of all particles (green solid) and the distribution of all particles crossing the transect (blue solid).

In summary, we have shown that the efficient and fast inshore route taken by the particles in late winter and spring corresponds to particles being advected within an intense northward laminar nearshore jet. In summer and autumn, the route

to St Helena Bay becomes less efficient and slower because of the offshore drift of the jet and its branching at Cape Columbine. Wind induced offshore Ekman transport contributes to particles being trapped within the offshore branches of the jet.

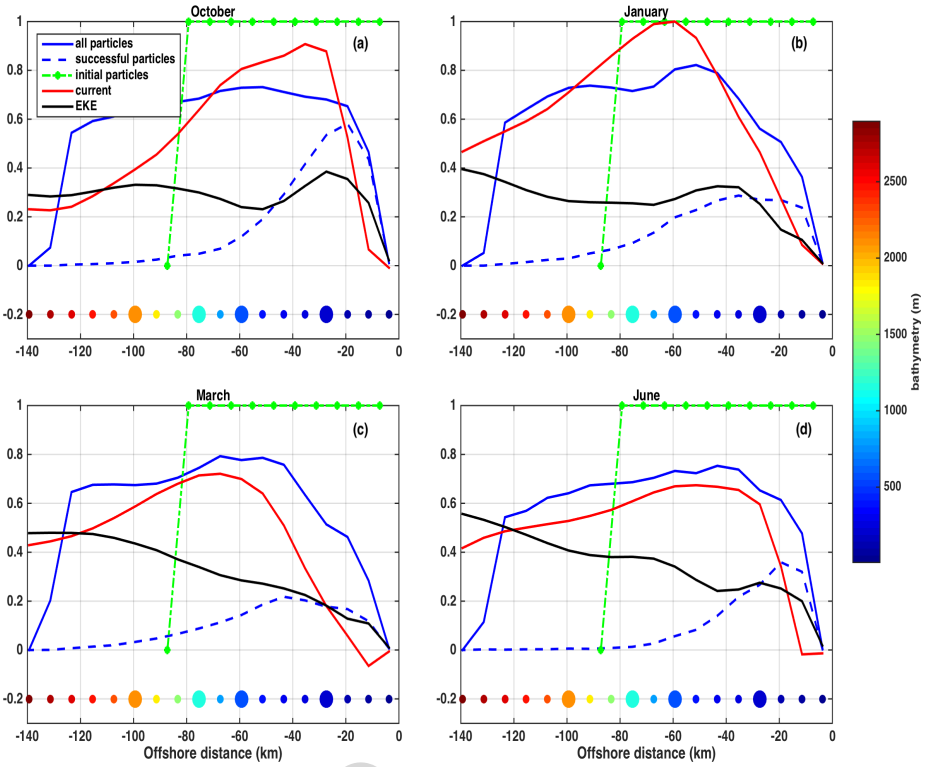

Figure 14: Across-shore profile of normalized depth-integrated alongshore current (red), EKE (black), and probability of the occurrence of particles (blue solid) at the SARP line. The histogram of successful particles is also superimposed (blue dashed) as well as the histogram of all particles at any release events (green solid). Profiles are plotted for: (a) October; (b) January; (c) March; (d) June. The depth-integrated alongshore current and EKE are computed over the top 100 m and then normalized by their maximum value found among the 12 monthly climatology across-shore profiles for all three transects. For the EKE, this maximum (0.07 m^2s^{-2}) occurred along the Grotto Bay transect in May. For the depth integrated current, this maximum (0.45 m s^{-1}) was found at the SARP line in January. The probability of occurrence of particles is normalized by its value on the SARP line when they are released. The colorbar shows the across-shore bathymetry, the enlarged circles mark the location of the 200 m, 500 m, 1000 m and 2000 m isobaths, respectively.

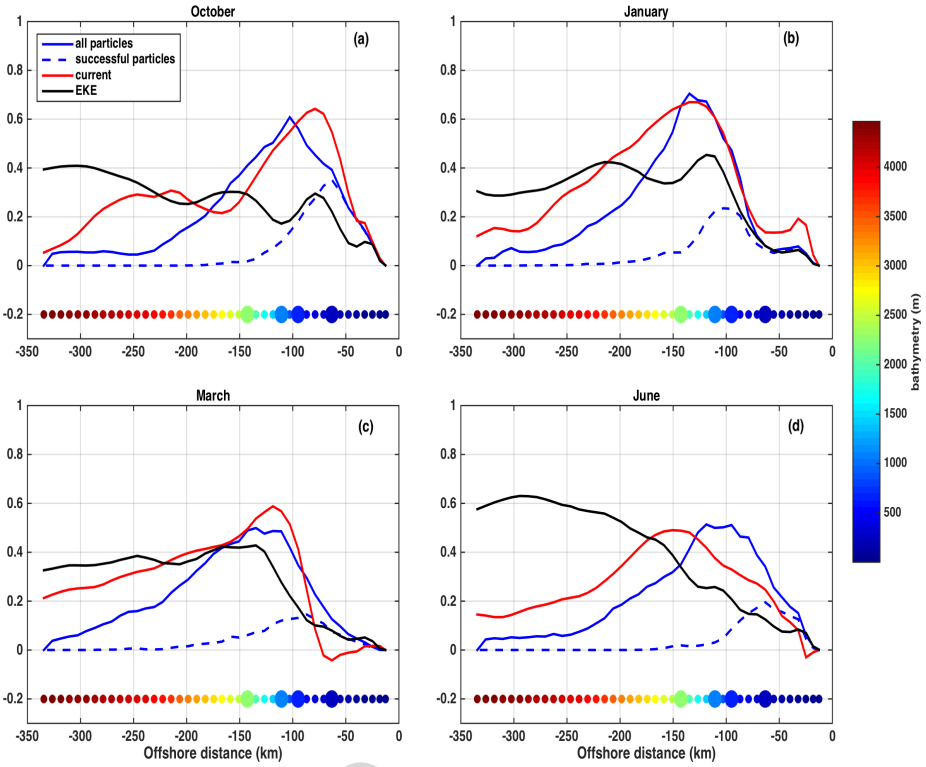

Figure 15: Same as Fig. 14 but for *Grotto Bay* (33.5° S).

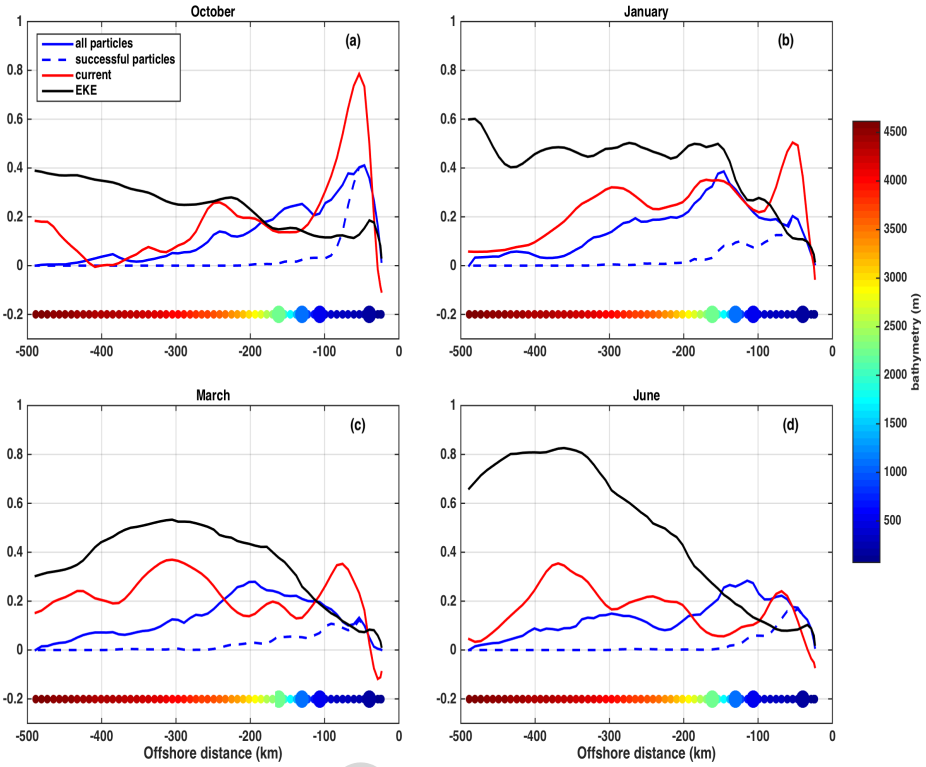

Figure 16: Same as Fig. 14 but for *Cape Columbine* (33° S).

5.2. Characteristics of the ocean circulation at depth

Surface alongshore currents have a complex across-shore structure (multiple jets), and show pronounced latitudinal contrasts in the intensity and position of the jets. In the following, we investigate how the vertical structure of the flow, associated with the multiple jets observed at the surface, may explain the sensitivity of transport success to the initial depth of particles (Fig. 9).

Vertical transects off Cape Point (not shown), Grotto Bay (Fig. 17) and Cape Columbine (not shown) all show the existence of a poleward undercurrent lying over the shelf slope. This poleward undercurrent seems to persist all year round, but has a strong seasonal cycle. In winter (June), it is weak ($\sim$5 cm s^{-1}), narrow

(∼40 km) and located deeper than 100 m depth. During the upwelling season, it is strong (∼25 cm s^{-1}), wider (∼100 km); its core extends in the offshore direction and towards the surface (≥50 m depth). The strengthening of the poleward undercurrent and its uplifting to the surface during austral summer is induced by the development of a negative (cyclonic) wind-stress curl within the 100 km nearshore band in relation to the coastal wind drop-off (Fig. 17).

The shoaling and strengthening of the poleward undercurrent impacts the surface currents. At the SARP line, it mainly induces an offshore shift of the alongshore northward jet, which leads to the occurrence of a surface counter current in the nearshore area. North of Cape Point, the strengthening of the poleward undercurrent comes with the vertical pinching and weakening of the surface current. Off Grotto Bay, in January, the core of the undercurrent domes so sharply that it almost outcrops the surface 100 km from the coast. This mechanism is responsible for the bifurcation and separation of the surface current into multiple jets. While the main branch of the northward surface jet remains located offshore and extends as deep as 500 m depth, the coastal branch is squeezed between the surface and 50 m depth and follows the 300 m isobath. This squeezing of the surface jet should cause particles released below 50 m depth to be embedded within the poleward undercurrent. Consequently they would fail to reach St Helena Bay. The cumulated transport success according to the depth of release (not shown) shows the opposite. It turns out that the successful particles progress northward after getting trapped within the core of the thick offshore branch of the current.

The processes impacting the particles located in the top 50 m of the water column can be explored by considering the ageostrophic velocities in the vertical across-shore transects off the west coast (Fig. 18). The latter are computed after subtracting the geostrophic velocity (derived from the hydrography) from

the total velocity. As expected, ageostrophic currents are found in the surface and bottom boundary layers. When the upwelling favourable winds prevail in summer, intense offshore velocities are found in the top 40 m due to the Ekman drift. Surface particles get advected offshore into a region of intensified mesoscale activity.

In EBUS, surface EKE generally increases as one goes offshore through the coastal transition zone but remains low at depths (Capet et al., 2008b). In the SBUS, intrusions of warm waters from the Agulhas Current in the form of eddies and filaments sustain high levels of EKE at depths (Veitch et al., 2009; Veitch and Penven, 2017). This high EKE pattern is generated by eddies and filaments being directly injected in the system from the Agulhas retroflection region and/or being formed from baroclinic/barotropic instabilities of the jet itself. This is clearly observable off Grotto Bay in winter, when the absence of upwelling allows these intrusions to progress near the coast (Fig.19). In summer, these intrusions still happen but progress more offshore, beyond the upwelling density front. However, peaks of surface EKE can still be observed within the top 100 m of the water column in the first 200 km nearshore band. These peaks are linked to barotropic/baroclinic instabilities of the different branches of the jet. One peak coincides with the offshore anticyclonic part of the surface jet, whereas the inshore peak coincides with the poleward undercurrent.

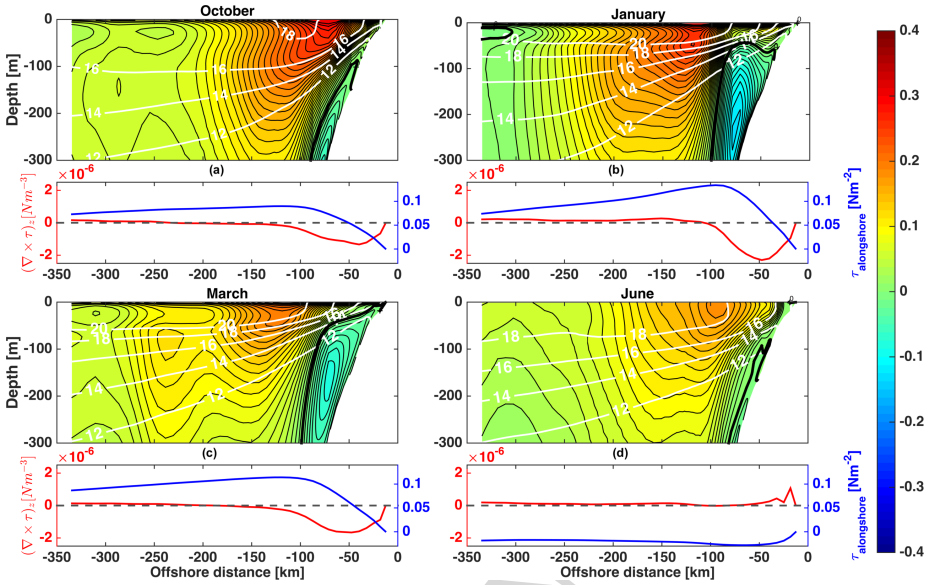

Figure 17: (Top): Grotto Bay vertical transect of alongshore velocities (color in m s^{-1}) and isotherms (white contours with contour spacing of 2°C). Contours of the current intensity are also superimposed (black) with a contour pacing of 1 cm s^{-1} and the zero contour in thick. (Bottom): The alongshore wind stress (blue) and z-component of the wind-stress curl (red) are superimposed for each across-shore transect, with the zero line (black dashed). Quantities are the monthly climatologies for: (a) October; (b) January; (c) March; (d) June.

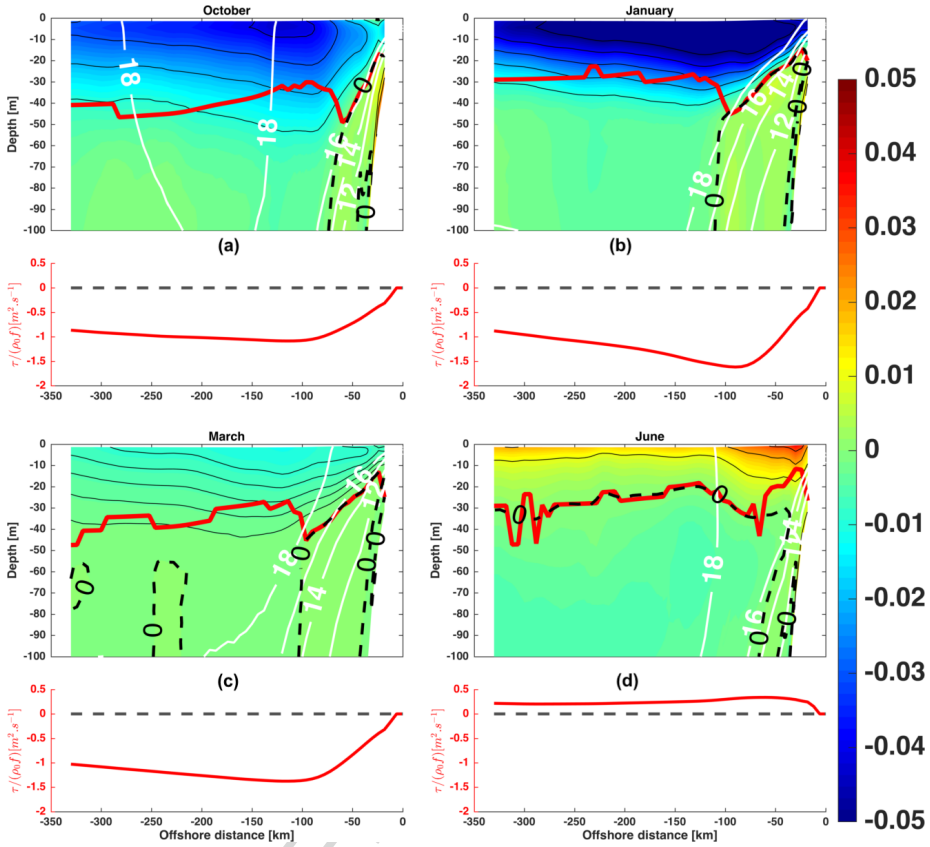

Figure 18: (Top): Grotto Bay vertical transect of across-shore ageostrophic velocities (color in m s^{-1}) and isotherms (white contours with contour spacing of 2°C). Contours of the current intensity are superimposed (black) with a contour spacing of 1 cm s^{-1} (zero contour in thick). The depth of the Ekman layer (m), computed after matching the vertical integration of the ageostrophic velocity with the total across-shore Ekman transport ($\tau_{alonsgore}/(\rho f)$) is also superimposed in red. (Bottom): The across-shore Ekman transport along each across-shore transect (red) , with the zero line (black dashed). Quantities are the monthly climatologies for: (a) October; (b) January; (c) March; (d) June.

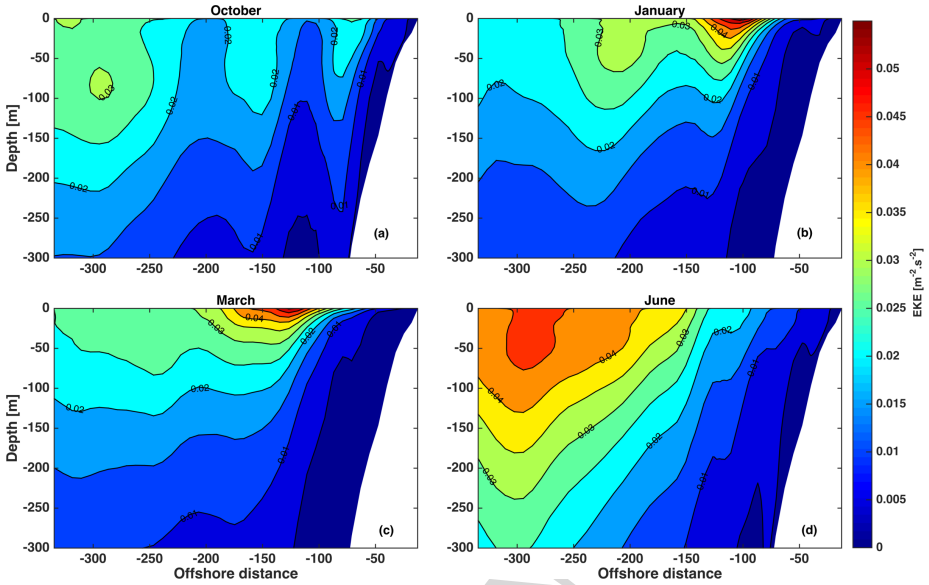

Figure 19: Grotto Bay vertical transect of monthly climatology of EKE (color in m^2 s^{-2}) for: (a) October; (b) January; (c) March; (d) June.

6. Discussion and conclusions

Lagrangian experiments, based on a 22 years (1989-2010) interannual simulation of the oceanic circulation in the SBUS, are used to describe the alongshore connectivity between Cape Point and St Helena Bay. Hutchings (1992) had previously pointed out the existence of an alongshore corridor followed by fish eggs and larvae that were spawn on the Agulhas Bank. A series of Lagrangian studies had then linked this corridor with the existence of the Benguela Jet, a shelf edge equatorward current (Blanke et al., 2009; Veitch et al., 2017).

This study confirms that successful particles leave the SARP line, *i.e.* the transect off Cape Point, and progress northward embedded within the Benguela Jet. Nevertheless, the latter intensifies during the upwelling season, while transport success decreases during this period. This brings to light that other dynam-

ical processes impact Lagrangian transports. Wind-induced across-shore Ekman transport, offshore mesoscale instabilities, Agulhas intrusions in the form of eddies and filaments combine together with the complex structure of the alongshore jets to transport particles towards St Helena Bay. The across-shore position of the jet, its intensity, its orientation relative to the coast and its bifurcation also play a key role and need to be taken into account when quantifying the alongshore connectivity.

We have shown that there is an efficient fast inshore route during late winter and early spring that is facilitated when the surface equatorward alongshore jet is in the form of one coherent intense nearshore branch. At this time of the year, transport success between Cape Point and St Helena Bay is at its highest rate (30%), and mainly involves particles initially released within the nearshore band delimited by the 300 m isobath: 90% of these latter particles are successfully transported to St Helena Bay in less than 15 days following a laminar route with little across-shore dispersion.

When the prevailing upwelling favourable winds start blowing consistently, transport success decreases continuously until it reaches its lowest value (15%) at the end of the upwelling season (March). Previous studies have attributed this decrease to an offshore loss of particles induced by a peak in the offshore wind induced Ekman drift. Our study shows that a reduced transport success can also be linked to a change in the structure of the equatorward jet. This occurs when the jet is shifted offshore towards a region of higher EKE, and particles are then more likely to fall within mesoscale features such as eddies or filaments and to get dispersed offshore. At this time of the year, the fast inshore successful route still exists, but becomes less likely than other offshore routes. Particles taking these offshore routes have a longer journey towards the target area (> 20 days). This study confirms that the offshore deviation of the Benguela Jet is linked

to the poleward undercurrent intensification and shoaling (Veitch et al., 2017). During the upwelling season, the wind drop-off within the first 100 km coastal band (due to the contrast in the land/sea drag coefficient) induces injection of negative cyclonic wind stress curl within the water column. The core of the poleward undercurrent thickens and outcrops to the surface, inducing the branching of the surface jet and/or a surface counter current in the nearshore band. This branching directly impacts the transport success, as successful particles follow the inshore branch. To do so, they must already be located within the inshore cyclonic side of the jet's core at the latitude of the jet's bifurcation. We have also shown that wind-induced Ekman surface drift acts on the particles either to keep them within the inshore side of the current in winter or to push them further offshore in summer.

In summary, our simulations identified an efficient inshore pathway taken by particles in spring. This period is the optimal window, as the jet is in its intensified state, close to the shore, and relatively stable. At this time of the year, offshore Ekman transport is still low enough to allow particles to remain on the inshore side of the jet. The core of the poleward undercurrent remains located deeper than 100 m depth and therefore does not trap any particles.

One may question the limitations of this work in terms of realism of the ocean circulation model, and argue about the robustness of our results if carried out with a higher resolution model. Increasing the model resolution may certainly lead to a better representation of the bathymetry, in particular in regions with steep slopes, which may in turn modify the jet's positions and intensity, and therefore impacts the absolute values of transport success. However, we believe that the seasonal cycle of transport success and the processes that lead to it would still hold.

The characteristics of the jet in the 7.5 km interannual simulation, with the

bifurcation and branching into multiple cores, are consistent with observations. The separation of the jet off Cape Columbine was pointed out in Fowler and Boyd (1998). Shannon and Nelson (1996) (their fig. 20) found a double-core jet off Cape Point. The two cores were respectively located over the 100 m and 300 m isobath and separated by the shoaling of a poleward undercurrent. Additionally, the seasonal cycle of transport success is intimately related to the seasonal cycle of the Benguela Jet itself. The latter is in thermal wind-balance with the across-shore temperature gradient. Coarser simulations, forced with a monthly seasonal climatology wind, already had the ability to reproduce the seasonal cycle of this gradient just because they could reproduce the seasonality of the coastal upwelling (Penven et al., 2001; Veitch et al., 2017). Lagrangian studies based on these simulations found a seasonal cycle of transport success similar to ours (Parada et al., 2003; Huggett et al., 2003; Mullon et al., 2005). The main difference concerned the winter particles that had a higher chance of reaching St Helena Bay than in our simulations (Huggett et al., 2003), probably because inshore Ekman transport kept particles within the inshore jet, and the latter had less seasonal variability.

Lagrangian experiments based on a higher resolution simulation are expected to provide new insights on the role of (sub-)mesoscale turbulence on the dispersion of particles. Future studies should analyse this variability in detail using a higher resolution ($\preceq$ 3 km) nested simulation embedded within the 7.5 km simulation described here. Combining a better resolution of the innershelf dynamics together with a high-frequency atmospheric forcing should also lead to a more subtle nearshore dynamics made of thin jets (Gan and Allen, 2002a,b) and inertial waves (Simpson et al., 20021; Lucas et al., 2014).

This study has helped us identify some of the physical processes important for the dispersal of fish larvae in the SBUS. Our results show that being entrained

within the fast inshore route taken by the Benguela Jet and avoiding being carried offshore when the jet splits into several branches are two major drivers of the connectivity between the spawning and nursery grounds. They must be considered as two important components of the fish reproductive strategy in the Southern Benguela. Finally, this study shows that successful transport from the Agulhas Bank to the west coast upwelling region cannot be attributed to only a simple wind induced modulation of the jet, as mentioned in previous studies. The seasonal characteristics of transport success result from the complex interactions of the Benguela Jet, the poleward undercurrent and the offshore Ekman transport together with the turbulent off-shelf eddy field.

To conclude, it is important to recall that if the Lagrangien particles used for this study were to be considered as living larvae, transport success to the nursery grounds by the oceanic currents is only one of the factors that contribute to their survival. Other physical properties such as water temperature, vertical stratification, small-scale turbulence also strongly influence the growth rate of larvae, as well as their survival by affecting the availability, distribution and composition of the prey and predator field.

Acknowledgements

The authors acknowledge the funding of N. Ragoasha' s PhD by the South-African National Research Foundation (NRF, South Africa) and the French Institute for Research and Sustainable Development (IRD, France). This work was also supported by the French national program LEFE/INSU under the project's name Benguela Upwelling Innershelf Circulation (BUIC). This work was granted access to the HPC resources of [TGCC/CINES/IDRIS] under the allocation 2017- [DARI n°A0020107443] attributed by GENCI (Grand Equipement National de Calcul Intensif).

References

Armstrong, D.A., Mitchell-Innes, B.A., Verheye-Dua, F., Waldron, H., Hutchings, L., 1987. Physical and biological features across an upwelling front in the southern Benguela. S. Afr. J. Mar. Sci. 5, 171–190. doi:10.2989/025776187784522559.

Bang, N., Andrews, W., 1974. Direct-current measurements of a shelf-edge frontal jet in southern benguela system. J. Mar. Res. 32, 405–417.

Beckmann, A., Haidvogel, D.B., 1993. Numerical simulation of flow around a tall isolated seamount. part i: Problem formulation and model accuracy. J. Phys. Oceanogr. 23, 1736–1753.

Blanke, B., Penven, P., Roy, C., Chang, N., Kokoszka, F., 2009. Ocean variability over the agulhas bank and its dynamical connection with the southern benguela upwelling system. Journal of Geophysical Research: Oceans 114. URL: https://agupubs.onlinelibrary.wiley.com/doi/abs/10.1029/2009JC005358, doi:10.1029/2009JC005358, arXiv:https://agupubs.onlinelibrary.wiley.com/doi/pdf/10.1029/2009JC005358.

Capet, X., Colas, F., Penven, P., Marchesiello, P., McWilliams, J.C., 2008a. Eddies in eastern boundary subtropical upwelling systems, in: Hecht, M.W., Hasumi, H.H. (Eds.), Ocean Modeling in an Eddying Regime. Washington, D. C.. volume 177.

Capet, X., McWilliams, J.C., Molemaker, M.J., Shchepetkin, A.F., 2008b. Mesoscale to Submesoscale Transition in the California Current System. Part I: Flow Structure, Eddy Flux, and Observational Tests. J. Phys. Oceanogr. 38, 29–43. doi:10.1175/2007JPO3671.1.

Carton, J.a., Giese, B.S., 2008. A Reanalysis of Ocean Climate Using Simple Ocean Data Assimilation (SODA). Mon. Weather Rev. 136, 2999–3017. doi:10.1175/2007MWR1978.1.

Castelao, R.M., Barth, J.A., 2007. The Role of Wind Stress Curl in Jet Separation at a Cape. J. Phys. Oceanogr. 37, 2652–2671. doi:10.1175/2007JPO3679.1.

Debreu, L., Marchesiello, P., Penven, P., Cambon, G., 2012. Two-way nesting in split-explicit ocean models: Algorithms, implementation and validation. Ocean Model. 49-50, 1–21. doi:10.1016/j.ocemod.2012.03.003.

Fairall, C.W., Bradley, E.F., Godfrey, J.S., Wick, G.A., Edson, J.B., Young, G.S., 1996. Cool-skin and warm-layer effects on sea surface temperature. J. Geophys. Res. 101, 1295–1308. doi:10.1029/95JC03190.

Fowler, J.L., Boyd, A.J., 1998. Transport of anchovy and sardine eggs and larvae from the western agulhas bank to the west coast during the 1993/94 and 1994/95 spawning seasons. S. Afr. J. Mar. Sci. 19, 181–195. doi:10.2989/025776198784127006.

Gan, J., Allen, J.S., 2002a. A modeling study of shelf circulation off northern California in the region of the Coastal Ocean Dynamics Experiment 2. Simulations and comparisons with observations. J. Geophys. Res. 107, 1–21. doi:10.1029/2001JC001190.

Gan, J., Allen, J.S., 2002b. A modeling study of shelf circulation off northern California in the region of the Coastal Ocean Dynamics Experiment: Response to relaxation of upwelling winds. J. Geophys. Res. 107, 6–31. doi:10.1029/2000JC000768.

Garavelli, L., Grüss, a., Grote, B., Chang, N., Smith, M., Verley, P., Stenevik,

E.K., Kaplan, D.M., Lett, C., 2012. Modeling the dispersal of Cape hake ichthyoplankton. Journal of Plankton Research 34, 655–669. doi:10.1093/plankt/fbs039.

Gordon, A., 1985. Indian-Atlantic transfer of thermohaline water at the Agulhas retroflection. Science 227, 1030–1033.

Gula, J., Molemaker, M.J., McWilliams, J.C., 2014. Submesoscale Cold Filaments in the Gulf Stream. J. Phys. Oceanogr. 44, 2617–2643. doi:10.1175/JPO-D-14-0029.1.

Huggett, J., Boyd, A.J., Hutchings, L., Kemp, A.D., 1998. Weekly variability of clupeoid eggs and larvae in the Benguela jet current: implications for recruitment. S. Afr. J. Mar. Sci. 19, 197–210. doi:10.2989/025776198784126773.

Huggett, J., Fréon, P., Mullon, C., Penven, P., 2003. Modelling the transport success of anchovy Engraulis encrasicolus eggs and larvae in the southern Benguela: The effect of spatio-temporal spawning patterns. Marine Ecology Progress Series 250, 247–262. doi:10.3354/meps250247.

Hutchings, L., 1992. Fish harvesting in a variable, productive environment searching for rules or searching for exceptions? S. Afr. J. Mar. Sci. 12, 297–318. doi:10.2989/02577619209504708.

Hutchings, L., Barange, M., Bloomer, S.F., Boyd, a.J., Crawford, R.J.M., Huggett, J.a., Kerstan, M., Korrûbel, J.L., de Oliveira, J.a.a., Painting, S.J., Richardson, a.J., Shannon, L.J., Schülein, F.H., van der Lingen, C.D., Verheye, H.M., 1998. Multiple factors affecting South African anchovy recruitment in the spawning, transport and nursery areas. S. Afr. J. Mar. Sci. 19, 211–225. doi:10.2989/025776198784126908.

Large, W.G., McWilliams, J.C., Doney, S.C., 1994. Oceanic vertical mixing: A

review and a model with a nonlocal boundary layer parameterization. Reviews of Geophysics 32, 363–403. doi:10.1029/94RG01872.

Lemarié, F., Kurian, J., Shchepetkin, A.F., Molemaker, M.J., Colas, F., McWilliams, J.C., 2012. Are there inescapable issues prohibiting the use of terrain-following coordinates in climate models? Ocean Modelling 42, 57 – 79. doi:10.1016/j.ocemod.2011.11.007.

Lett, C., van der Lingen, C., Loveday, B., Moloney, C., 2015. Biophysical models of larval dispersal in the benguela current ecosystem. African Journal of Marine Science 37, 457–465. doi:10.2989/1814232X.2015.1105295.

Loveday, B.R., Durgadoo, J.V., Reason, C.J., Biastoch, A., Penven, P., 2014. Decoupling of the Agulhas leakage from the Agulhas Current. Journal of Physical Oceanography , 140411151744003doi:10.1175/JPO-D-13-093.1.

Lucas, A.J., Pitcher, G.C., Probyn, T.A., Kudela, R.M., 2014. The influence of diurnal winds on phytoplankton dynamics in a coastal upwelling system off southwestern Africa. Deep Sea Res., Part II 101, 50–62. doi:10.1016/j.dsr2.2013.01.016.

Marchesiello, P., Debreu, L., Couvelard, X., 2009. Spurious diapycnal mixing in terrain-following coordinate models: The problem and a solution. Ocean Modelling 26, 156–169. doi:10.1016/j.ocemod.2008.09.004.

Marchesiello, P., McWilliams, J.C., Shchepetkin, A., 2001. Open boundary conditions for long-term integration of regional oceanic models. Ocean Modell. 3, 1–20.

Marchesiello, P., Shchepetkine, A.F., McWilliams, J.C., 2003. Equilibrium structure and dynamics of the California Current System. J. Phys. Oceanogr. 126, 753–783.

Mullon, C., Fréon, P., Parada, C., Van Der Lingen, C., Huggett, J., 2003. From particles to individuals: Modelling the early stages of anchovy (Engraulis capensis/encrasicolus) in the southern Benguela. Fish. Oceanogr. 12, 396–406. doi:10.1046/j.1365-2419.2003.00240.x.

Mullon, C., Fron, P., Cury, P., 2005. The dynamics of collapse in world fisheries. Fish and Fisheries 6, 111–120. doi:10.1111/j.1467-2979.2005.00181.x.

Nelson, G., 1989. Poleward motion in the Benguela area, in Poleward Flows Along Eastern Ocean Boundaries. Springer, New York.

Nelson, G., Hutchings, L., 1983. The Benguela upwelling area. Prog. Oceanog. 12, 333–356. doi:10.1016/0079-6611(83)90013-7.

Pagès, F., Verheye, H.M., Gili, J.M., Flos, J., 1991. Short-term effects of coastal upwelling and wind reversals on epiplanktonic cnidarians in the Southern Benguela ecosystem. South African Journal of Marine Science 10, 203–211. doi:10.2989/02577619109504632.

Parada, C., Mullon, C., Roy, C., Fréon, P., Hutchings, L., Van Der Lingen, C.D., 2008. Does vertical migratory behaviour retain fish larvae onshore in upwelling ecosystems? A modelling study of anchovy in the southern Benguela. African Journal of Marine Science 30, 437–452. doi:10.2989/AJMS.2008.30.3.1.635.

Parada, C., Van Der Lingen, C.D., Mullon, C., Penven, P., 2003. Modelling the effect of buoyancy on the transport of anchovy (Engraulis capensis) eggs from spawning to nursery grounds in the southern Benguela: An IBM approach. Fish. Oceanogr. 12, 170–184.

Penven, P., Debreu, L., Marchesiello, P., McWilliams, J.C., 2006. Evaluation and application of the ROMS 1-way embedding procedure to the central cal-

ifornia upwelling system. Ocean Model. 12, 157. doi:10.1016/j.ocemod.2005.05.002.

Penven, P., Marchesiello, P., Debreu, L., Lefèvre, J., 2008. Software tools for pre- and post-processing of oceanic regional simulations. Environmental Modelling and Software 23, 660–662. doi:10.1016/j.envsoft.2007.07.004.

Penven, P., Roy, C., Lutjeharms, J., Colin de Verdière, A., Johnson, A., Shillington, F., Fréon, P., Brundrit, G., 2001. A regional hydrodynamic model of the Southern Benguela. S. Afr. J. Mar. Sci. 97, 472–476.

Piollé, J., Autret, E., 2011. Product user manual for l3 and l4 odyssea sst products over the global and north wertern shelves. Myocean.

Saha, Suranjana, e.a., 2010. The ncep climate forecast system reanalysis. Bull. Amer. Meteor. Soc. 91, 1015–1057. doi:10.1175/2010BAMS3001.1.

Shannon, L., Nelson, G., 1996. The Benguela: large scale features and processes and system variability, in: Wefer, G., Berger, W.H., Shiedler, G., Webb, D. (Eds.), The South Atlantic. Present and past circulation. Springer-Verlag, Berlin Heidelberg, pp. 163–210.

Shannon, L.V., 1985. The benguela ecosystem. i. evolution of the bengue]a, physical features and processes. In Oceanography and Marine Biology , 105–182.

Shchepetkin, A.F., McWilliams, J.C., 1998. Quasi-monotone advection schemes based on explicit locally adaptive dissipation. Mon. Weather Rev. 126, 1541–1580. doi:10.1175/1520-049.

Shchepetkin, A.F., McWilliams, J.C., 2005. The regional oceanic modeling system (ROMS): A split-explicit, free-surface, topography-following-coordinate

oceanic model. Ocean Model. 9, 347–404. doi:10.1016/j.ocemod.2004.08.002.

Shelton, P.A., Hutchings, L., 1982. Transport of anchovy, engraulis capensis gilchrist, eggs and early larvae by a frontal jet current. Journal du Conseil 40, 185–198. doi:10.1093/icesjms/40.2.185.

Shelton, P.A., Hutchings, L., 1990. Ocean stability and anchovy spawning in the southern benguela current region. Fish. Bull. 88, 323–338.

Simpson, J.H., Hyder, P., Rippeth, T.P., Lucas, I.M., 20021. Forced oscillations near the crtitical latitude for diurnal-inertial-resonnance. J. Phys. Oceanogr. 32, 177–187.

Skogen, M.D., Shannon, L.J., Stiansen, J.E., 2003. Drift patterns of anchovy engraulis capensis larvae in the southern benguela, and their possible importance for recruitment. Afr. J. mar. Sci. 25, 37–47. doi:10.2989/18142320309503999.

Smith, W.H.F., Sandwell, D.T., 1997. Global sea floor topography from satellite altimetry and ship depth soundings. Science 277, 1956–1962. doi:10.1126/science.277.5334.1956.

Twatwa Mhlongo, N., van der Lingen, C., Drapeau, L., Moloney, C., Field, J., 2005. Characterising the spawning habitats of anchovy engraulis encrasicolus and sardine sardinops sagax in the southern benguela upwelling ecosystem. Afr. J. mar. Sci. 27, 487–500.

Veitch, J., Florenchie, P., Shillington, F., 2006. Seasonal and interannual fluctuations of the angola-benguela frontal zone (abfz) using 4.5 km resolution satellite imagery from 1982 to 1999. Int. J. Remote Sens. 27, 987–998. doi:10.1080/01431160500127914.

Veitch, J., Hermes, J., Lamont, T., Penven, P., Dufois, F., 2017. Shelf-edge jet currents in the southern benguela: A modelling approach. J. Mar. Sys. doi:10.1016/j.jmarsys.2017.09.003.

Veitch, J., Penven, P., Shillington, F., 2009. The Benguela: A laboratory for comparative modeling studies. Prog. Oceanog. 83, 296–302. doi:10.1016/j.pocean.2009.07.008.

Veitch, J.A., Penven, P., 2017. The role of the Agulhas in the Benguela Current system: A numerical modeling approach. J. Geophys. Res. 122, 3375–3393. doi:10.1002/2016JC012247.

Highlights

- Fish larvae pathways in the Southern Benguela Upwelling System
- A 300 miles along shore fast route for fish larvae in the Southern Benguela
- Lagrangian pathways in the Southern Benguela Upwelling System